1.4 Experimental Study of Thermocapillary Flow in the Half-Zone Liquid Bridge of Low Prandtl Number Fluid

Space Utilization Research Center

National Space Development Agency of Japan

Experimental Study of Thermocapillary flow in the Half-Zone Liquid Bridge of Low Prandtl Number Fluid

Ryoji IMAI, Katsuhiko TAKAGI, Masahiko OOTAKA,
Fumiaki OOTSUBO, Hidesada NATSUI, and
Shinichi YODA

Abstract

In the research presented herein, thermal and hydrodynamic behaviors in a low Pr number liquid were investigated by experiment, numerical analysis, and linear stability analysis to clarify the transition mechanism toward oscillatory thermocapillary flow. In this section, we describe experimental studies in the half zone liquid bridge of a low Prandtl number liquid such as Sn molten material. Temperature fluctuations on the free surface of the liquid bridge are measured before detecting the transition point toward the oscillatory thermocapillary flow.

Experimental equipment for observing and measuring thermocapillary flow was comprised of a vacuum chamber, a melt supplying chamber, an *in-situ* observation system, and a vacuum measurement system.

Molten tin, selected for its low melting point and low vapor pressure, provided the specimens for these experiments. Two pure iron columns, between which little chemical reaction will occur even when wet, were used to form and sustain the liquid bridge on ground.

Thermocapillary flows were confirmed by tracing the slug generated naturally on a free surface, and temperature fluctuations were detected by IR imager. The minimum frequency of temperature fluctuation was 0.56Hz on a liquid bridge of 10mm in diameter and 4.5mm in height at a temperature difference of 20K.

1 Introduction

It is well known that thermocapillary flow has an undesirable effect on the crystal growth of semi-conductors by the floating zone (FZ) method, which leads to striation of the dopant induced by oscillatory thermocapillary flow in melt.

Many experimental researches, numerical simulation, and theoretical analyses have been conducted on thermocapillary flow in the half zone-liquid bridge, using simulated molten material in the FZ configuration. These previous researches proved that flow and temperature fields were governed by dimensionless parameter of Marangoni or Reynolds number defined as following:

$$Ma = \frac{\left|\frac{\partial \sigma}{\partial T}\right| \Delta T a}{\mu \alpha} \quad ; \text{Marangoni number}$$

$$Re = Ma / Pr \quad ; \text{Reynolds number}$$

a: radius of liquid bridge, Pr: Prandtl number, ΔT: temperature difference
α: thermal diffusivity, μ: viscosity

Thermocapillary flow would be transitioned from axisymmetric steady flow to 3D oscillatory flow as the temperature difference increased. Figure 1-1 shows an overview of the transition behavior of thermocapillary flow. In a high Prandtl number liquid, it was proved that thermocapillary flow transitions from axisymmetric steady flow to 3D oscillatory flow occur beyond the onset point. On the other hand, it was found that thermocapillary flow in a low Prandtl number liquid had two transition points; that is, a flow transition from axisymmetric flow to 3D steady flow occur at the first bifurcation point, and a flow transition from 3D steady flow to 3D oscillatory flow occurs at the second bifurcation point. To date, transition phenomena in low Prandtl number liquids have been investigated primarily by linear stability analysis and numerical simulation.

Most previously documented experiments have dealt with transparent liquid of a high Pr number in ambient temperature; it is easy to handle such a liquid and to observe its flow field. In contrast, experiments with a low Pr number liquid have been few. This is due to

following reasons:

(1) Low Pr number liquid is opaque. Its flow field cannot be observed in bulk by means of a visual ray.

(2) High temperature liquids such as metals and alloys are difficult to handle and oxidize easily.

(3) An oxidation film suppresses thermocapillary flow.

Figure 1-2 shows the influence of the Prandtl number on the critical Reynolds number obtained by linear stability analysis and direct numerical simulation. In the case of tin with Prandtl number of 0.01, 5.0 mm height, and unity in aspect ratio, the temperature difference at the first and second bifurcation point is about 1.6K and 5.3K, respectively. These values are much smaller compared to those for high Prandtl number materials.

Table 1-1 shows a list of previous experiments using low Prandtl number liquid. It should be noted that most experiments were carried out for the purpose of studying crystal growth ; that is, experiments focused on whether oscillatory flow would produce impurity in striation during crystal growth. To date, few observations and measurements of flow and temperature have been conducted in low Prandtl number materials.

Nakamura and Hibiya [1], [2] measured temperature at the free surface by means of thermocouple and flow velocity by tracking some particle movements observed by X-ray in a molten silicon column of 10 mm in diameter. Frequency of temperature fluctuation was 0.1Hz at a temperature difference of 100K. However, the half-zone configuration was not completed, and, thus, the heat flux was applied across the free surface as well as on the rod at the top or bottom of the liquid bridge. Therefore, precise comparison cannot be made with past numerical calculations.

Han J., et al. [3] experimentally investigated thermocapillary convection in the liquid bridge of mercury. Free surface fluctuations were measured by non-contacted diagnostic method, and they found the critical Marangoni number, detecting it to be 900 with an oscillatory frequency around 5Hz. However, since they used copper rods to sustain the liquid bridge, a copper-mercury amalgam was generated on the free surface, which leads to formation of a skin and free surface pollution.

Kou S., et al. [4] measured temperature fluctuation on the free surface in molten silicon of 13mm in diameter by pyrometer. According to their measurement, a frequency of 0.07Hz and an amplitude of 4K were obtained at Marangoni number of 6200. According to the

numerical results in Imaishi's calculation, frequency of temperature fluctuation is in the order of 10^{-1}Hz even for much lower Marangoni numbers: 0.44 Hz accompanies Marangoni number of 226.

Various theoretical and numerical analyses have been conducted in low Pr number liquid. Kuhlmann [5] and Chen [6] investigated transition phenomena by using linear stability theory. They showed that thermocapillary flow transitioned from axisymmetric steady flow to 3D steady flow beyond the critical Reynolds number Re_{cr}, and investigated the influence of the aspect ratio of the liquid bridge, heat loss from the free surface, buoyancy convection, and so on. Rupp & Muller [7], Levenstam [8], Kuhlmann [9], and Imaishi [10] conducted direct numerical analyses, and found that there existed second bifurcation points in addition to the that of the above transition from 3D steady flow to oscillatory 3D flow.

Rarely has the critical Marangoni number been successfully determined by an experimental approach in low Prandtl number liquid.

The overall purpose of the present study is to understand transition phenomena in molten materials by means of an experimental approach. We located a low Prandtl number liquid among molten metal and solid materials being capable of sustaining a liquid bridge on the ground. We constructed experimental equipment for observing and measuring thermocapillary flow, which was comprised of a vacuum chamber, a melt supplying chamber, and various systems for measurement. Thermocapillary flow was confirmed by observing slug movement on the free surface, and surface temperature fluctuation was detected by an IR imager. The minimum frequency of temperature fluctuation was 0.56Hz on the liquid bridge with a 10mm diameter and a height of 4.5mm at a temperature difference of 20K.

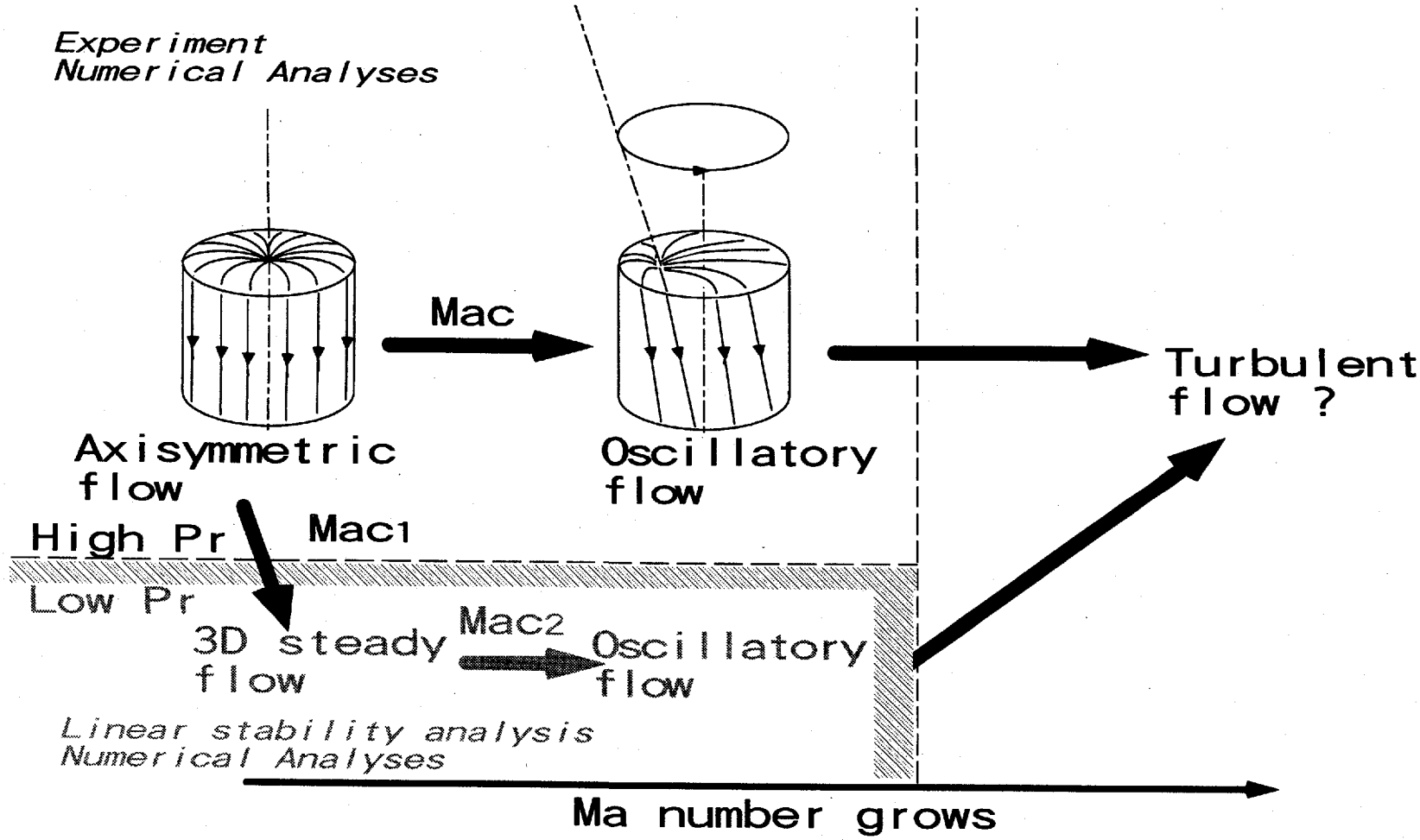

Figure 1-1. Transition phenomena of thermocapillary flow

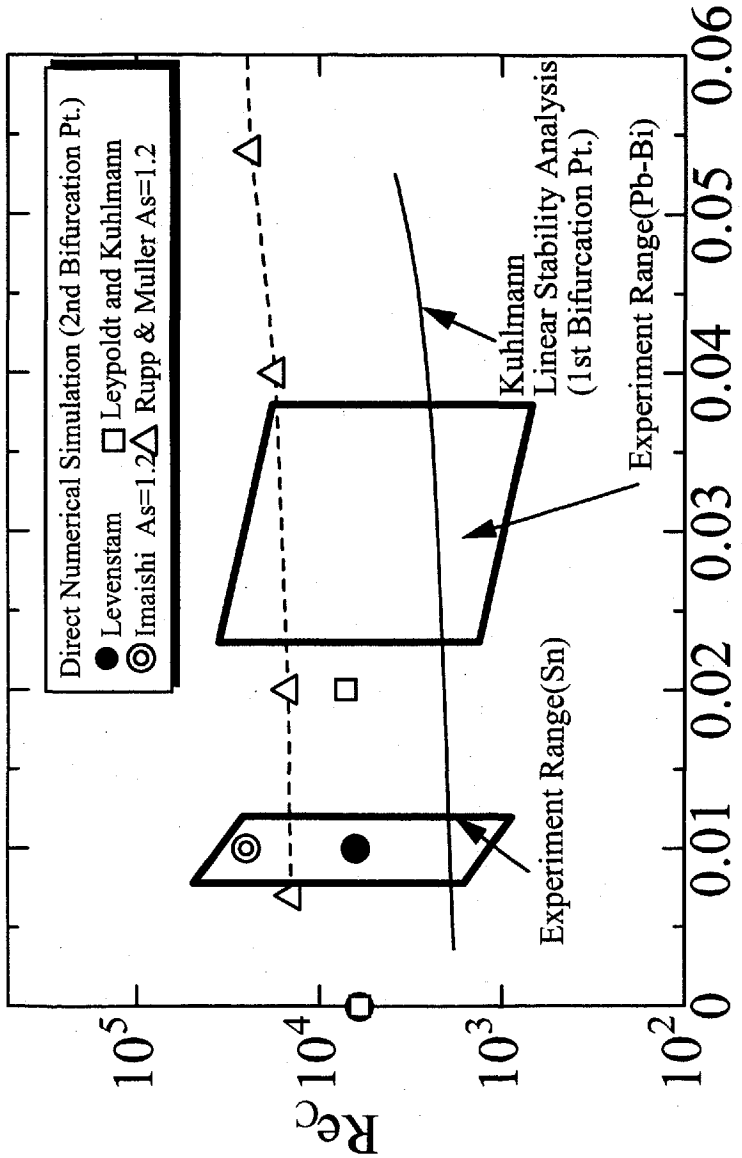

Figure 1-2. Pr number versus critical Reynolds number in low Prandtl number liquid

Table 1-1. List of experiments in low Prandtl number liquid

Year	Title	Author	General Description	Paper	Experiment
1983	Experiment on the thermocapillary convection of a mercury liquid bridge in a floating half zone	J.H. Han, W.R. Hu	Liquid bridge of mercury was used. Critical Ma was obtained by detecting surface deformation.	Journal of crystal growth 169(1996)129-135	1g
1989	The Floating-Zone Growth of Ti3Au and Ti3Pt	Y. K. Chang	Ti3Pt crystal was used. Surface striations was observed due to Marangoni convection.	Journal of crystal growth 62(1983)627-632	1g
1990	Floating zone growth of silicon under microgravity in a sounding rocket	A. Eyer, R. Nitsche	Si crystal was used. Surface striations was observed due to Marangoni convection.	Journal of crystal growth 71(1985)173-182	μg
1990	Transition from steady to time-dependent Marangoni convection in partially coated silicon melt zone	A. Croll, R. Nitsche	Si crystal was used. Surface striations was observed due to Marangoni convection. Critical Ma was 100-200.	Proc. VIIth European Symposium on Materials and Fluid Sciences in Microgravity, ESA SP-295	1g, μg
1990	Analysis of periodic non-rotational W striations in Mo single crystals due to nonsteady thermocapilary convection	M. Jurisch, W. Loser	W doped Mo crystal was used. Diameter dependence of critical Ma was obtained.	Journal of crystal growth 102(1990)214-222	1g
1996	Surface temperature oscillations of a floating zone resulting from oscillatory thermocapillary convection	M. Jurisch	Mo and Nb crystal was used. Surface striation and surface temperature fluctuation was measured. The frequencies by both measurements agreed. Electron beam heating facility was used.	Journal of crystal growth 102(1990)223-232	1g
1996	Experimental and numerical studies of thermocapillary convection in a floating zone like configuration	M. Levenstam, M Andersson	Si crystal was used. Temperature fluctuations near free surface was measured. Temperature fluctuation was seen. Numerical calculations were conducted.	Journal of crystal growth 158(1996)224-230	1g
1996	Thermocapillary convection in a low-Pr material under simulated reduced gravity	M. Cheng, S. Kou	Molten Si was used. Temperature fluctuation on free surface was measured by pyrometer. At Ma of 6200; temperature difference of 50K, oscillation 0.07Hz and 4K in amplitude was observed.	Proc. of 4th microgravity fluid physics & transport phenomena conference, 1998	1g
1998	Thermocapillary convection in a low-Pr material under simulated reduced gravity conditions	Y. Tao, S. Kou	Molten tin was used. Temperature fluctuation was measured by T/C. At temperature difference of 85K, oscillation of 5Hz and 1.3K in amplitude was observed.	Proc. of 2nd microgravity fluid physics & transport phenomena conference, 1996	1g
1998	Temperature fluctuations of the Marangoni flow in a liquid bridge of molten silicon under microgravity on board the TR-IA-4 rocket	S. Nakamura, T. Hibiya	Molten Si was used. Temperature fluctuation near free surface was measured by T/C. At melting process, 0.1Hz of temp. fluctuation was observed. In 1g, 0.2Hz was obtained.	Journal of Crystal Growth 186(1998) 85-94	1g, μg

2 Selection of low Prandtl number liquid and rod material

We investigated low Prandtl number liquids among molten metals to select a source of specimens for the experiments. A low melting point is preferable because temperature conditions can be easily controlled and maintained. To prevent oxidation of the free surface and heat loss from the free surface, the liquid bridge is preferably formed in a vacuum condition. Therefore, the vapor pressure of the liquid must be very low in order to minimize loss of volume due to vaporization.

Table 2-1 shows the investigated thermal properties of various liquid metals [11], [12]. We selected molten tin as liquid bridge material because its melting point is relatively low and its vapor pressure is extremely low.

Molten lead-bismuth alloy, which has been considered for a coolant of a Fast Breeder Reactor, was also selected because its melting point, 398.7K, is low; and its thermal properties have been thoroughly investigated. Table 2-2 shows the previously investigated thermal properties of molten eutectic lead-bismuth alloy [12], [13]. A notable advantage of this liquid is the low temperature coefficient of its surface tension, $d\sigma / dT = 4.0 \times 10^{-5}$ N/m/K ($d\sigma / dT = 7.0 \times 10^{-5}$ N/m/K in molten tin). This means that the temperature difference at the first and second bifurcation points is relatively larger: $\Delta T_{C1} = 6.7\,\mathrm{K}$, $\Delta T_{C2} = 16.9K$.

Now we considered the properties of the solid material, which sustains the liquid bridge, in terms of the chemical reactivity of the liquid against the solid. Slight chemical reactivity against the solid is required to obtain a stable liquid bridge. However, extreme chemical reactivity may lead to formation of an alloy melt between the liquid and the solid, and to changes in the thermal properties of the liquid during an experiment. We investigated for a solid that had proper wettability against molten tin with reference to the phase diagram. Figure 2-1 shows the phase diagrams of tin against copper and iron. The copper-tin diagram shows that the gradient of liquidus is gentle at the copper rich region and the atomic ratio of the liquid phase is about 8% at 773K, leading to the formation of an alloy between copper and tin. In contrast, the gradient of liquidus, as shown in the tin-iron phase diagram, is very sharp. Therefore, it was expected that the wettability of iron against molten tin was sufficient, and that negligible alloy formation would occur during an experiment. Based on these observations, we selected iron as the solid material to sustain the liquid bridge of molten tin.

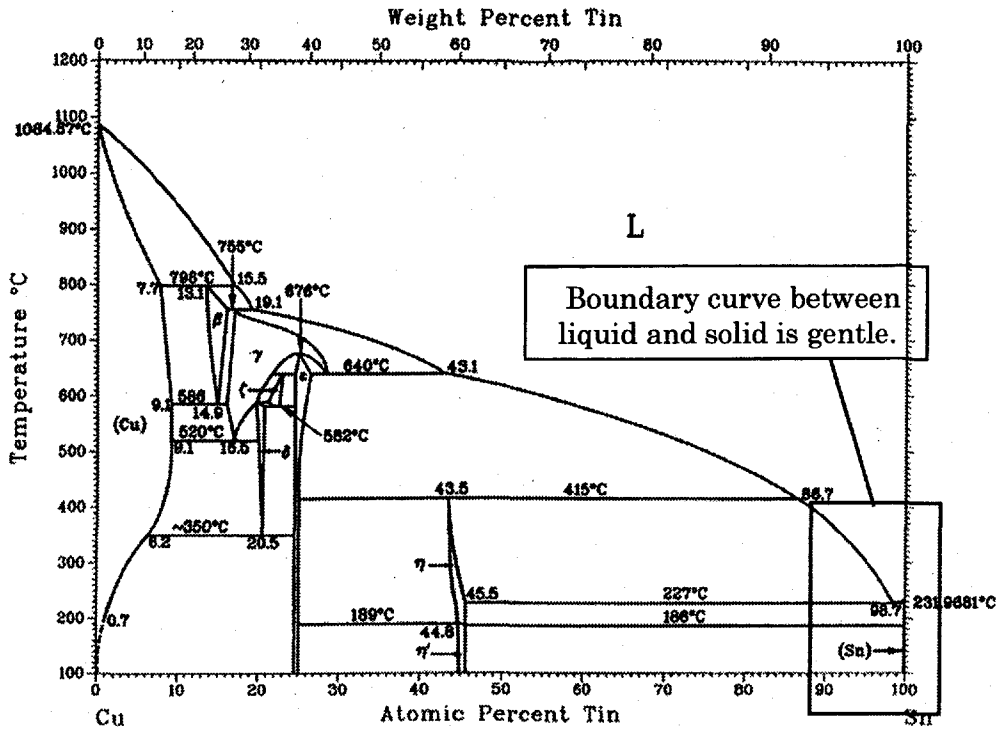

(a) Tin versus copper

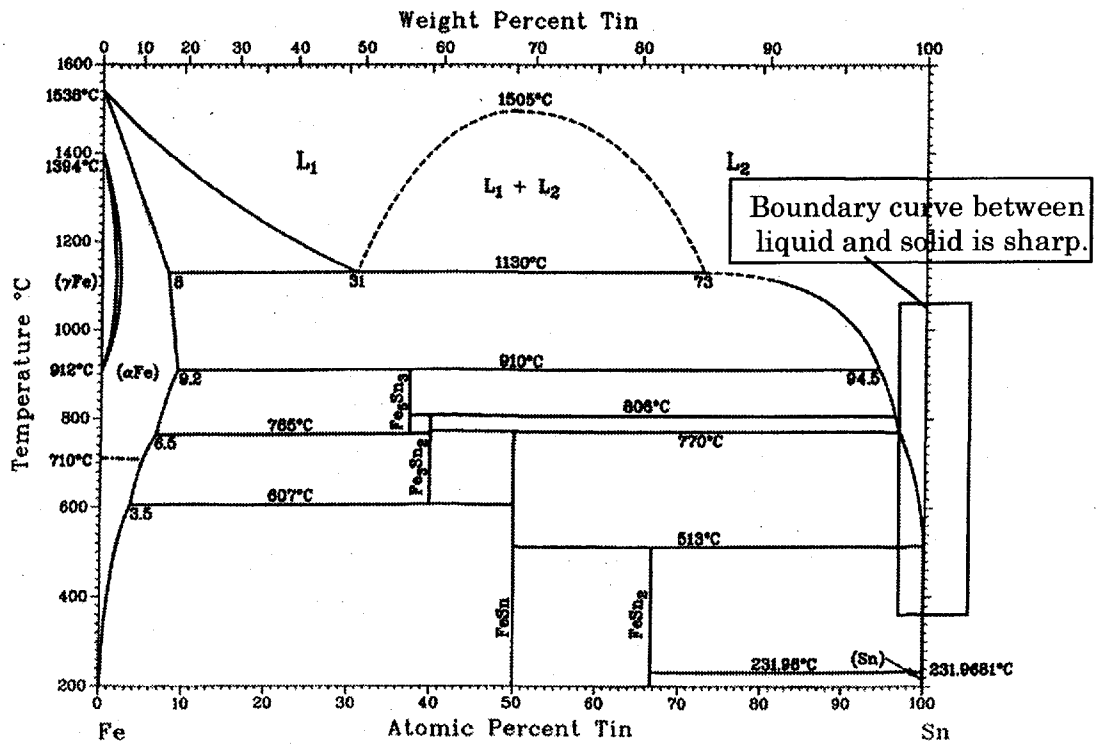

(b) Tin versus iron

Figure 2-1. Phase diagram

Table 2-1. Thermal properties of liquid metal

Material	Melting point [K]	Property @ melting point Density [kg/m3]	Dynamic Viscosity [m2/s]	Thermal conductivity [W/m/K]	Surface tension [N/m]	dσ/dt [N/m2]	Prandtl number	Vapor Pressure [kPa]
Pottasium (K)	337.00	8.293E+02	6.300E-07	5.820E+01	1.130E-01	6.200E-05	7.230E-03	3.130E-3(@400K)
Rubidium (Rb)	313.00	1.479E+03	3.730E-07	3.270E+01	8.910E-02	5.200E-05	6.370E-03	1.690E-4(@400K)
Caesium (Cs)	302.00	1.479E+03	3.510E-07	1.840E+01	7.030E-02	5.000E-05	8.330E-03	3.830E-4(@400K)
Mercury (Hg)	234.00	1.443E+04	1.500E-07	6.780E+00	4.650E-01	2.049E-04	3.833E-02	0.140 (@400K)
Tin (Sn)	505.00	6.830E+03	3.968E-07	3.000E+01	6.210E-01	2.056E-04	2.258E-02	3.320E-19(@600K)
Lithium (Li)	454.00	5.147E+02	1.145E-06	4.280E+01	3.983E-01	1.600E-04	6.050E-02	8.210E-10(@500K)
Sodium (Na)	371.00	9.252E+02	7.120E-07	9.110E+01	1.979E-01	9.100E-05	1.030E-02	1.840E-7 (@400K)
Gallium (Ga)	302.95	6.100E+03	3.344E-07	2.550E+01	7.160E-01	1.000E-04	3.184E-02	
Indium (In)	429.75	7.023E+03	2.691E-07	4.200E+01	5.560E-01	9.000E-05	1.166E-02	
Lead (Pb)	600.45	1.065E+04	2.178E-07	1.540E+01	4.420E-01	1.167E-04	2.290E-02	1.030E-7 (@700K)
Bismuth (Bi)	544.52	1.060E+04	1.670E-07	1.100E+01	3.900E-01	7.000E-05	2.100E-02	4.380E-10(@600K)

Table 2-2. Investigated thermal properties of molten eutectic lead-bismuth alloy

Temperature [K]	Density [kg/m3]	Dynamic Viscosity [m2/s]	Thermal conductivity [W/m/K]	Specific heat [J/kg/K]	Surface tension [N/m]	Evaporation pressure [Pa]	Prandtl number
400.00	1.057E+04	3.200E-07	1.090E+01	1.460E+02			4.500E-02
500.00	1.045E+04	2.330E-07	1.190E+01	1.460E+02			2.900E-02
600.00	1.033E+04	1.770E-07	1.290E+01	1.460E+02			2.100E-02
623.00					4.218E-01		2.100E-02
693.00					4.036E-01		2.100E-02
753.00					3.973E-01		2.100E-02
800.00	1.009E+04	1.320E-07	1.490E+01	1.460E+02			1.300E-02

3 Measurement of wettability

It is required that wettability between the liquid and the rod material should be sufficient to form a stable liquid bridge. The wettability is considered to depend on temperature because the chemical activity of the liquid against the rod material will be higher with increase in temperature. Therefore, we investigated the effect of temperature on wettability. We utilized the growing drop method, as shown in Fig. 3-1. Melt is formed in the BN cylinder by the heat from a halogen lamp, and discharged through a pinhole 0.5mm in diameter.

First, we investigated the wettability of molten tin against solid iron. Figure 3-2 shows the temperature dependence of the contact angle immediately after forming a tin droplet. This figure shows that the contact angle decreases with temperature. It is suggested that the reactivity of molten tin is higher with increasing temperature. Formation of a stable liquid bridge requires that the contact angle be less than 90deg. Figure 3-2 suggests that temperature during the experiment should be greater than 673K.

Next, we measured the contact angle of molten lead-bismuth alloy against sold iron. Figure 3-3 shows the temperature dependence of the contact angle immediately after forming a droplet of molten lead-bismuth alloy. The contact angle is larger than that of molten tin at the same temperature; this suggests that a temperature of 773K or more is required for a contact angle of at least 90deg. However, it was difficult to maintain pressure of even 10^{-3} torr at 773K due to vaporization of molten lead-bismuth alloy, which indicates that the volume of the liquid bridge of molten lead-bismuth alloy decreased under this temperature condition. Therefore, we investigated wettability against other solid candidates.

Figure 3-4 shows temperature dependence of the contact angle of molten lead-bismuth alloy against solid copper. It is found that the contact angle is smaller than that of solid iron, and it is expected that a stable liquid bridge is formed at the temperature of 573K or more.

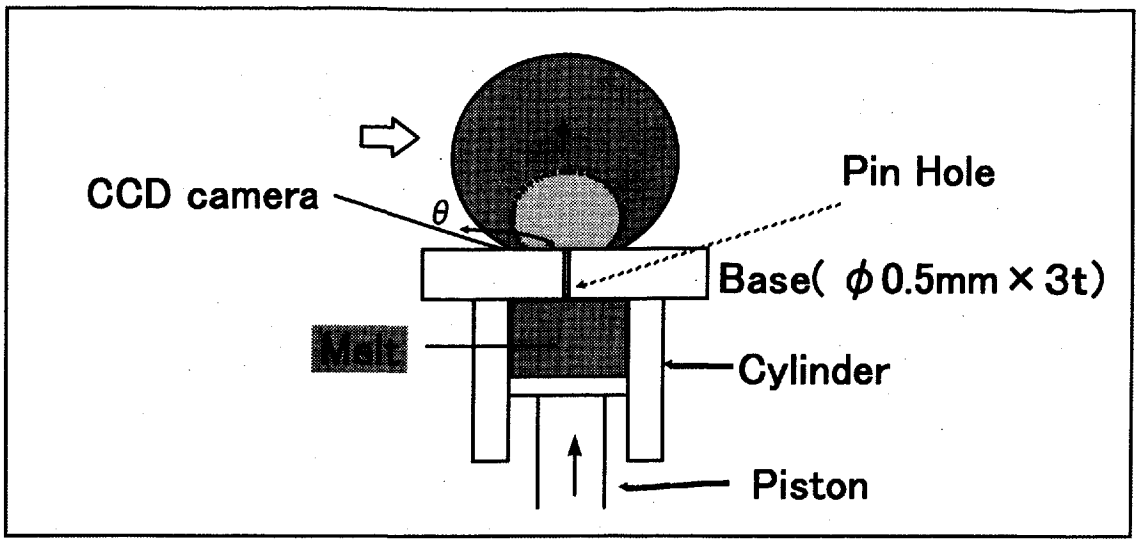

Figure 3-1. Growing drop method

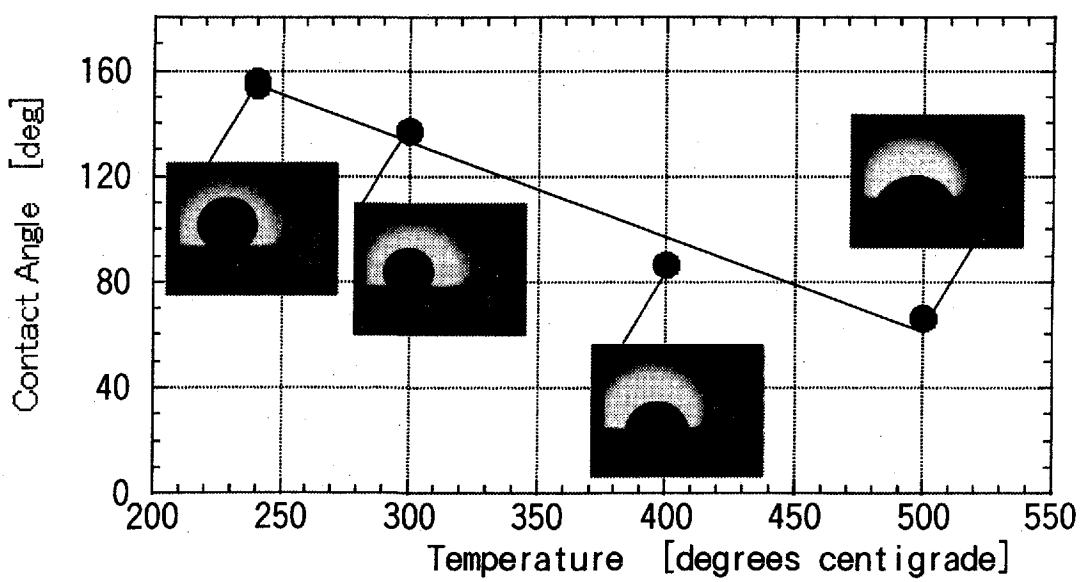

Figure 3-2. Temperature dependent of wettability

(Liquid: molten tin, Solid: iron)

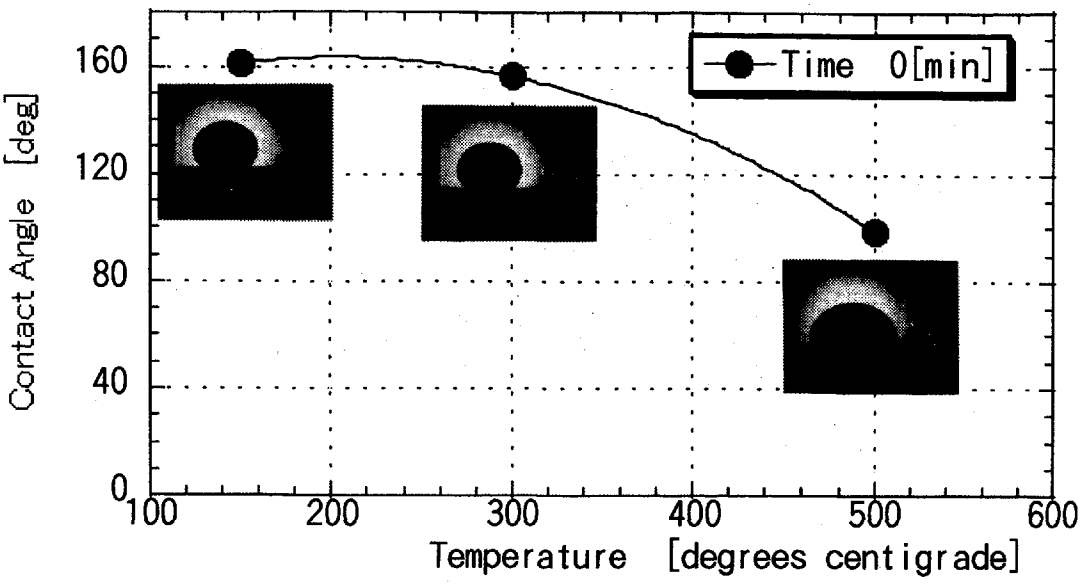

Figure 3-3. Temperature dependent of wettability

(Liquid: molten lead-bismuth alloy, Solid: iron)

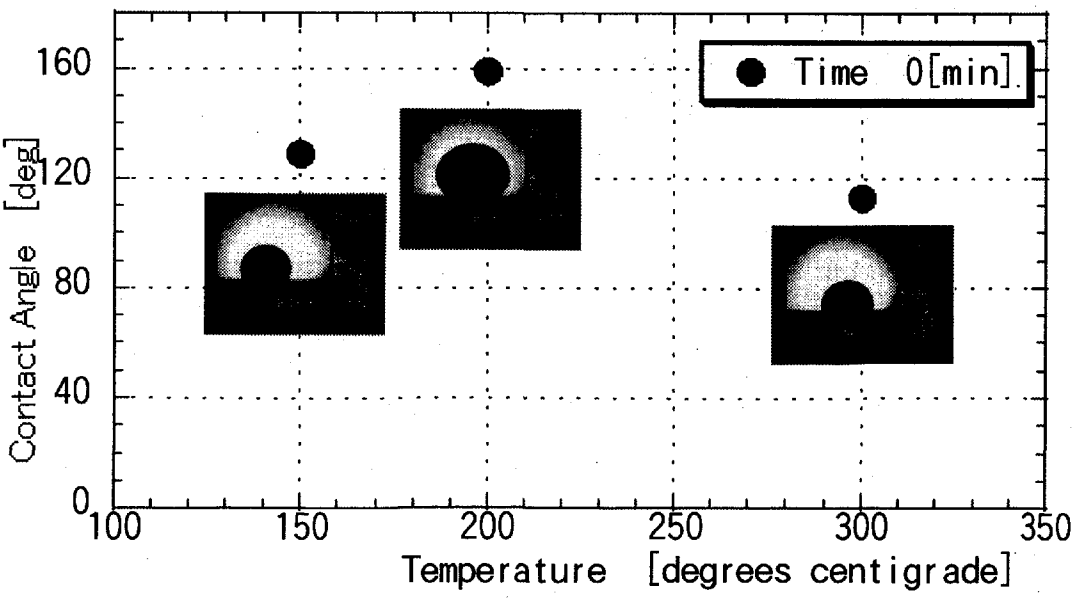

Figure 3-4. Temperature dependent of wettability

(Liquid: molten lead-bismuth alloy, Solid: copper)

4 Experimental device

The experimental apparatus was comprised mainly of a vacuum chamber, vibration proof table, melt supplying chamber, and systems for measurement. Diameter of the vacuum chamber was about 200mm, with a height of 400mm. Figure 4-1 shows the experimental apparatus and Fig. 4-2 shows the melt supplying chamber. The melt supplying chamber was 63.5mm in diameter and 290mm in height. The vibration proof table has a mechanism to isolate vibrations, which affect free surface fluctuation and flow in melt. The size of this table was 1000mm x 1500mm x 800mm.

The liquid bridge was formed in a vacuum chamber to prevent oxidation on the free surface, since oxidation film suppresses thermocapillary flow. In addition, nonevaporable getters (Japan Getters Incorporated HS405), which absorb residual oxide and vapor water, were installed near the liquid bridge.

Molten tin was supplied from the melt supplying chamber. This chamber consists of cylindrical containers with an electric heater and a pair of quartz containers; with the upper/lower container connected by a quartz throat and quartz capillary (see Fig. 4-2). Solid tin shot was inserted in the upper quartz container and melted by electric heater. The slug, *i.e.* tin oxides, was scratched at the quartz throat while molten tin drops moved down toward the lower quartz container by gravitational force. In addition, the slug adheres to the inner surface of the quartz capillary. Molten tin with a very small quantity of slugs was supplied to the vacuum chamber throughout these processes.

The liquid bridge is held between a pair of iron rods. These rods are heated by electric heater. The power of each rod heater is controlled independently, and the temperature of each rod is set up by PID controller.

The high reflectivity of the tin surface demands special attention to reduce radiation energy reflected on the surrounding objects. Because the rod heaters raise the temperature on the chamber wall by radiation, the chamber wall is cooled down by a water cooler. At the same time, cylindrical reflection panels are installed around the rod heaters to protect them from the radiated heat flux. In addition, the reflectivity of the inner chamber wall was reduced to prevent the reflection of heat flux on chamber wall. The inner chamber wall was coated with black paint.

Figure 4-3 shows the systems for measurement. Temperature fields on the surface of the liquid bridge are obtained by infrared thermal imaging radiometer (IR imager,

Inframetrics Inc. Model 760), and temperature in iron rods and ambient temperature are both measured by a K-type thermocouple. Temperature field is measured through a transparent Zn-Se window 8-12 μ m in wave length.

An optical heterodyne displacement meter (Photon Probe, Inc. HV-350) detected surface deformations of the liquid bridge. These data are accumulated in a personal computer *via* A/D converter, and analyzed simultaneously by data processing software.

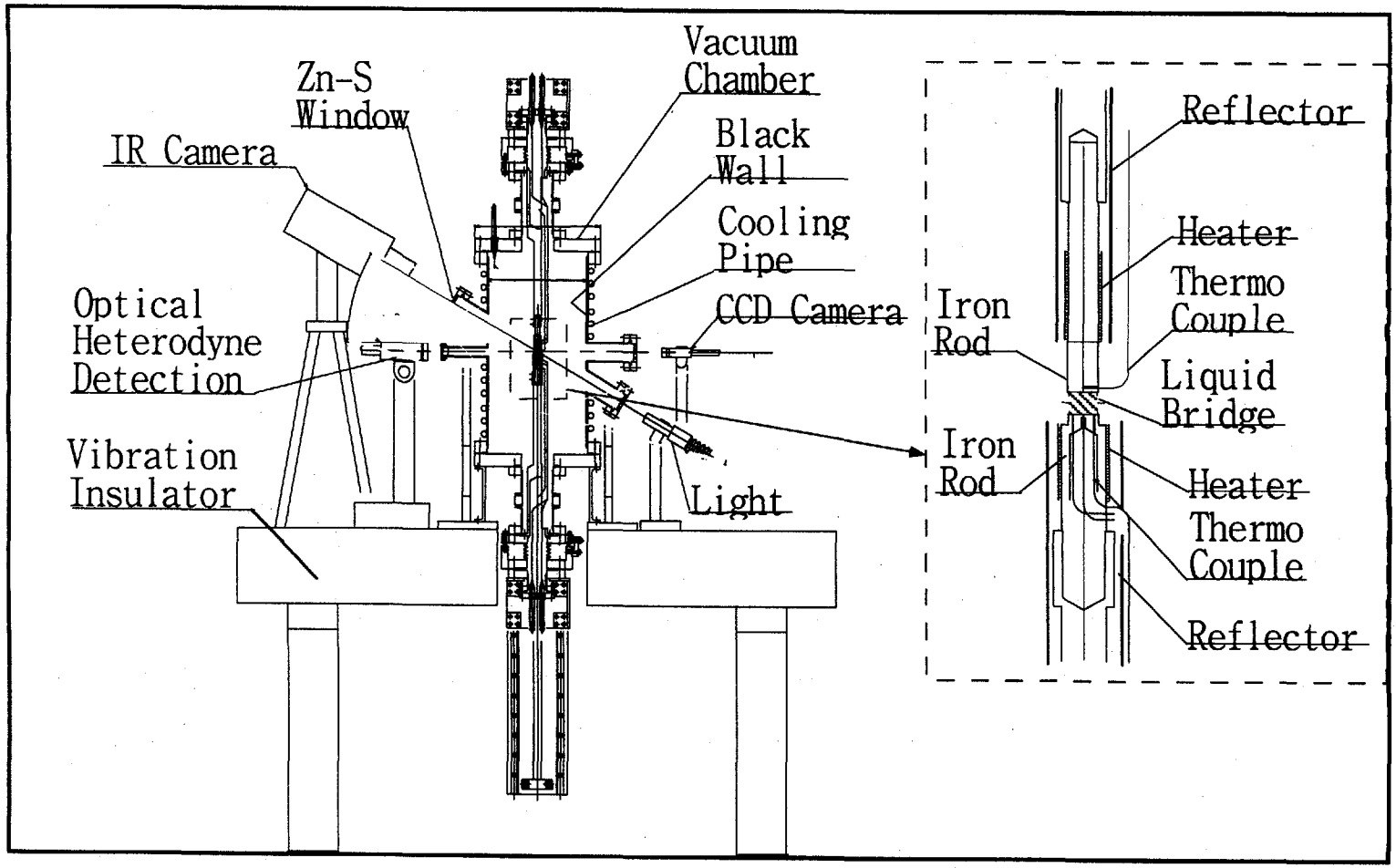

Figure 4-1. Schematic drawing of experimental apparatus

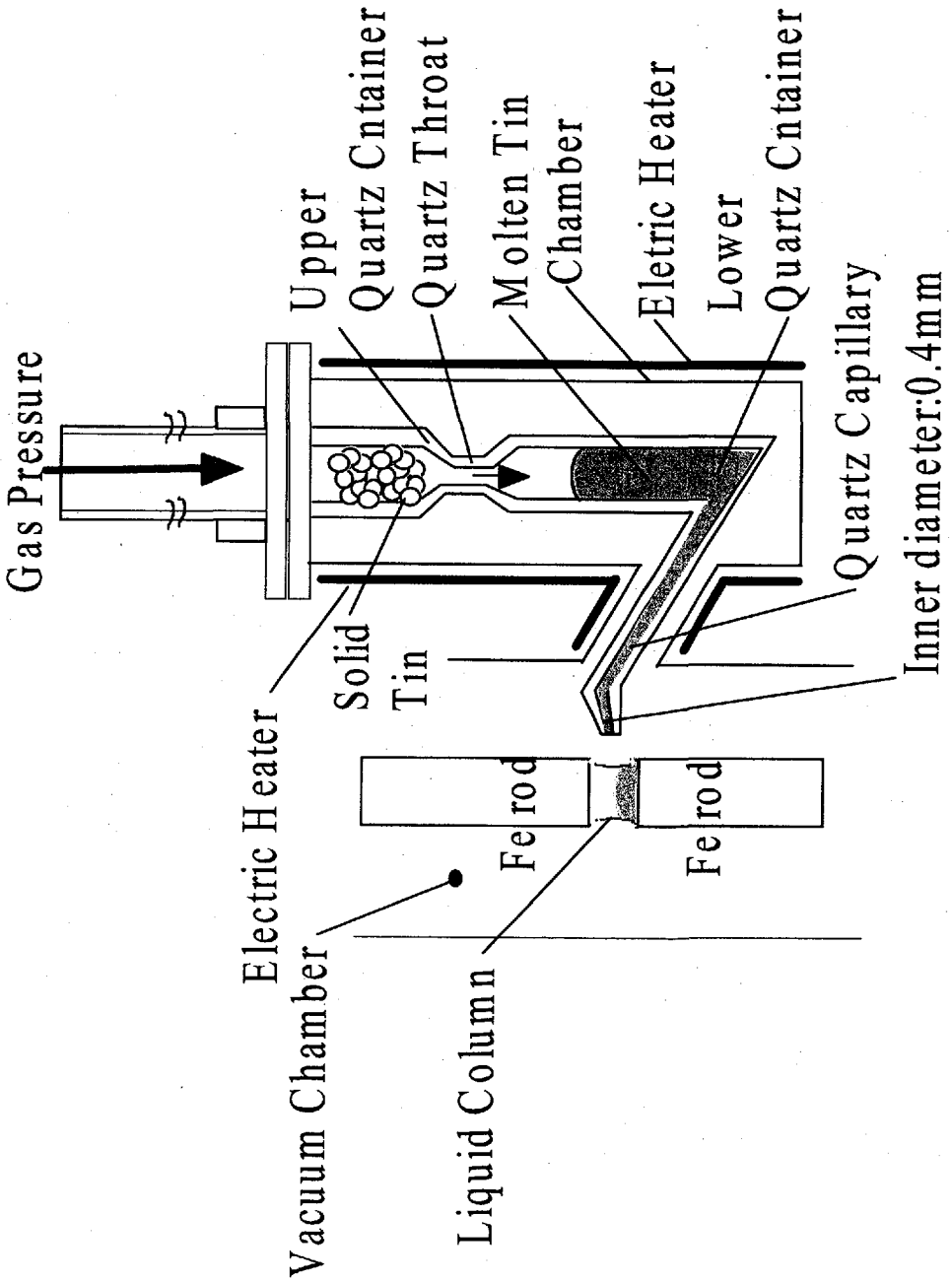

Figure 4-2. Melt supplying chamber

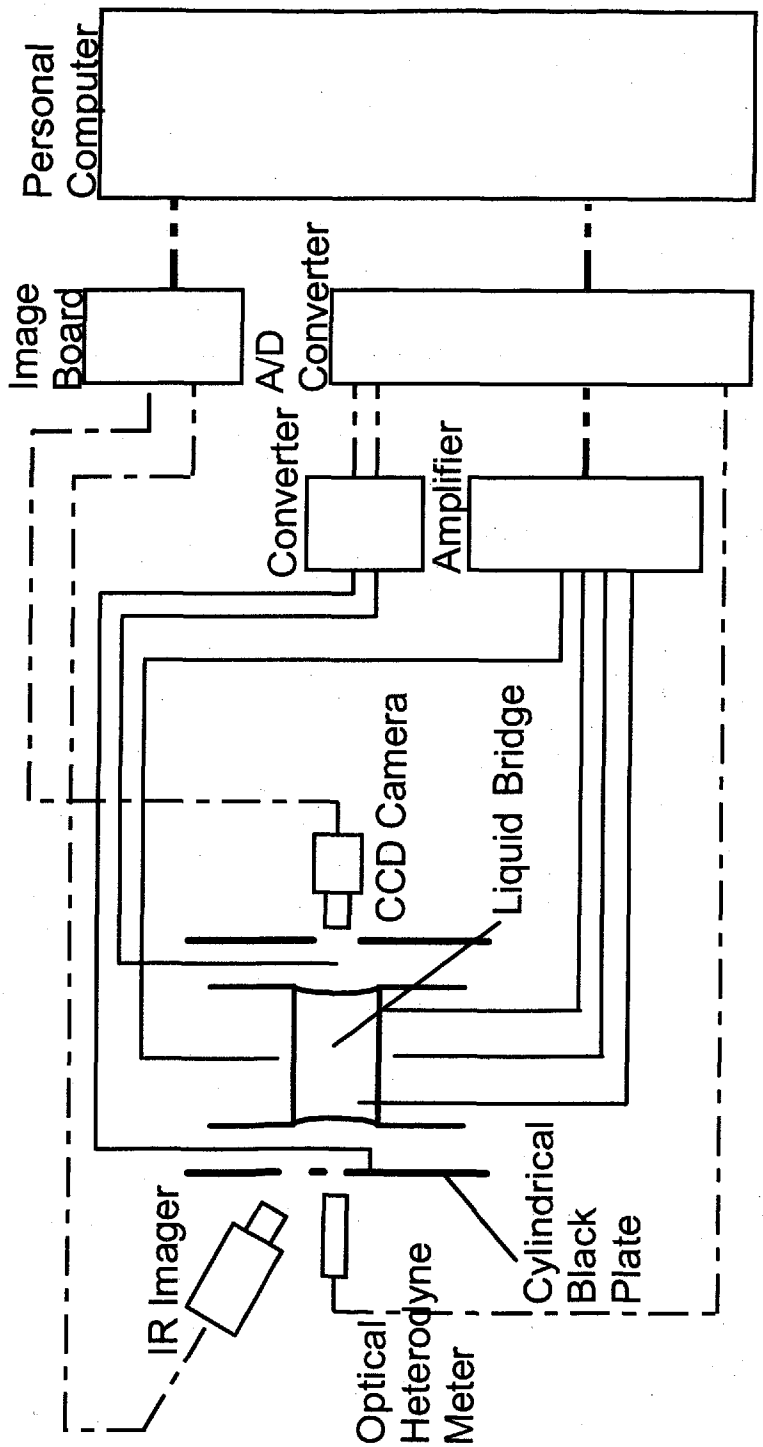

Figure 4-3. Measurement system

5 Formation of the stable liquid bridge

We investigated the dimensions of the liquid bridge, which we can form under ground gravity conditions. We calculated the meniscus of the liquid bridge considering gravitational force. Figure 5-1 shows a system of coordinates for calculating the meniscus of the liquid bridge. Governing equations include the following:

Balance between pressure difference and surface tension

$$p_0 - p = \sigma\left(\frac{1}{R_1} + \frac{1}{R_2}\right) \tag{5.1}$$

p : static pressure p_0 : referenced static pressure R_1, R_2 : main curvature

σ : surface tension]

Sum of main curvature is given as follows:

$$\frac{1}{R_1} + \frac{1}{R_2} = \pm\left(\frac{d\beta}{ds} + \frac{1}{r}\frac{dz}{ds}\right) \tag{5.2}$$

r, s, z, β : coordinating system, see Fig. 5-1.

Local pressure is due to gravitational force,

$$grad(p) = -\rho grad(gz) \tag{5.3}$$

g : gravitational acceleration

We obtain the differential equation from equations (5-1) to (5-3), and calculated these equations by the finite differential method.

Figure 5-2 shows the meniscus of molten tin to be 10mm in diameter and 5 and 10mm in height. A meniscus with 10mm in height has a significant distortion, and predicted that this liquid bridge would demonstrate difficulty sustaining a stable shape. On the other hand, we saw a slight distortion of the meniscus with 5mm in height. This liquid bridge would be expected to remain stable.

Figure 5-3 shows the meniscus of molten lead-bismuth alloy 10mm in diameter and 2.5 and 5mm in height. We find that a meniscus with 5mm in height has a significant distortion,

and that a meniscus with 2.5mm in height nearly exhibits a slight shape. The liquid bridge 2.5mm in height would be expected to remain stable.

Figure 5-4 shows a liquid bridge formed under ground gravity conditions. We changed the height of the liquid bridge in order to investigate stability at a range of heights, and found that a stable liquid bridge is obtained in each case.

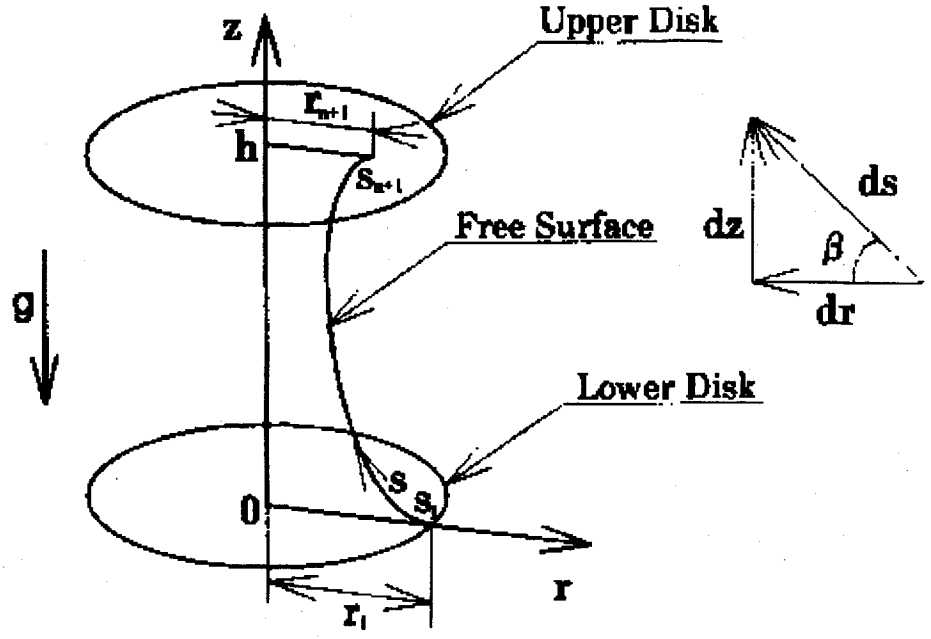

Figure 5-1. Calculation for meniscus of liquid bridge

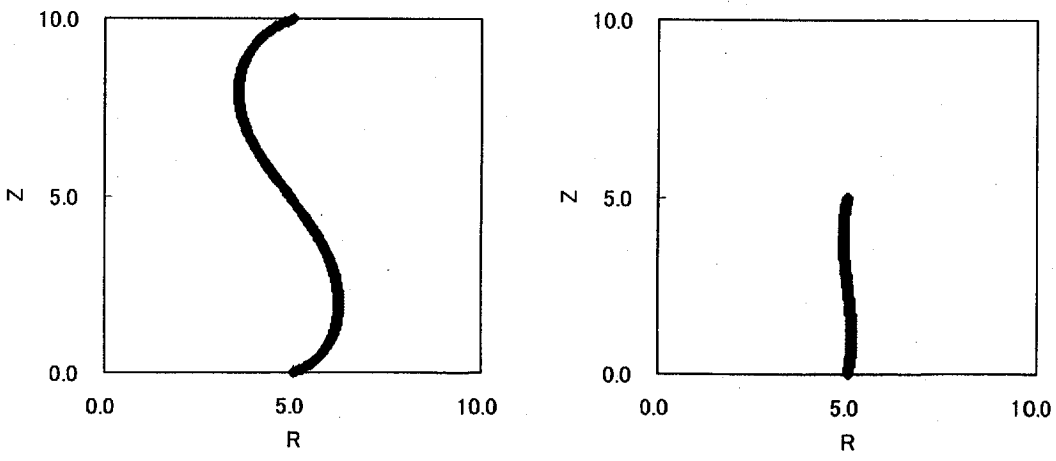

(a) 10 mm in diameter, 10 mm in height (b) 10 mm in diameter, 5 mm in height

Figure 5-2. Meniscus of molten tin

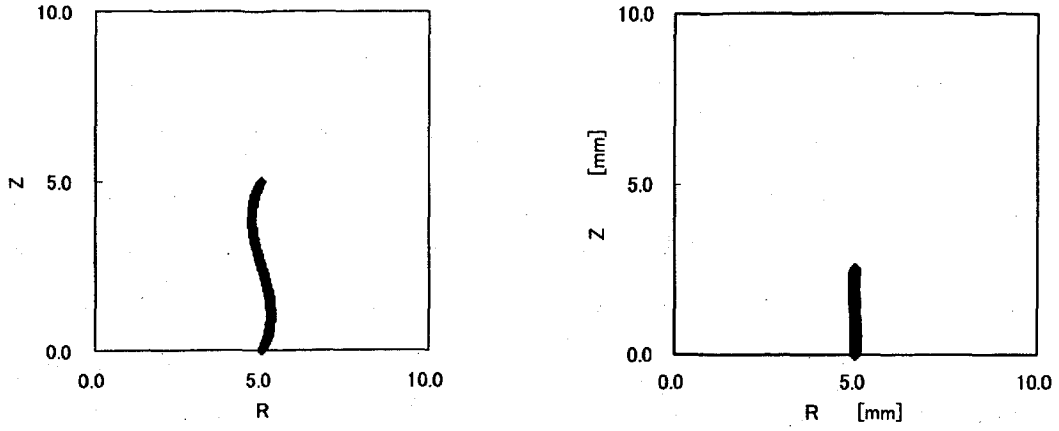

(a) 10mm in diameter, 5mm in height (b) 10mm in diameter, 2.5mm in height

Figure 5-3. Meniscus of molten lead-bismuth alloy

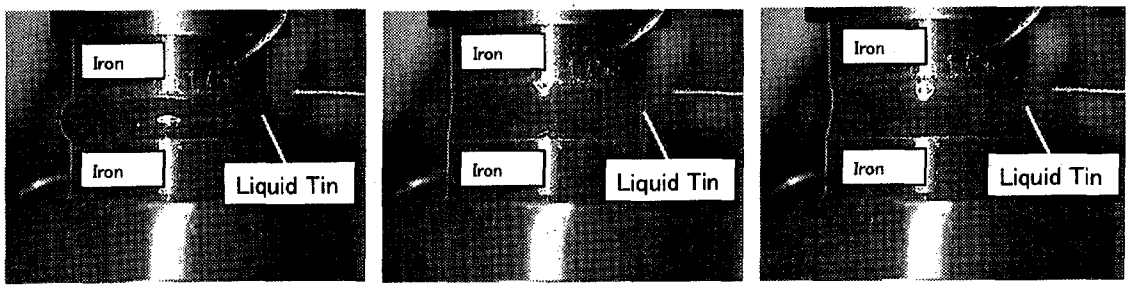

V/V0>1 V/V0~1 V/V0<1

Figure 5-4. Liquid bridge formed under ground gravity condition

(Effect of volume ratio)

6 Confirmation of Thermocapillary flow

We attempted to confirm thermocapillary flow by tracing a slug generated on the free surface. Figure 6-1 shows the movement of slugs on the free surface. Here, the degree of the vacuum is in the order of 10^{-5} Pa, the temperature of the upper and lower rods was 520K and 500K, respectively. The liquid bridge was 10mm in diameter and 8mm in height. We observed downward movement of the slug on the free surface. Since the density of the slug is less than that of the molten liquid, the slug will rise in the absence of downward flow. No buoyancy convection occurs since the temperature at the upper rod is higher than that at the lower rod, and the free surface is thermally insulated. Based on these observations, downward movement of a slug at liquid column surface implies that surface flow occurs due to thermocapillary effect. Under these conditions described above, we consider that thermocapillary effect generates this movement.

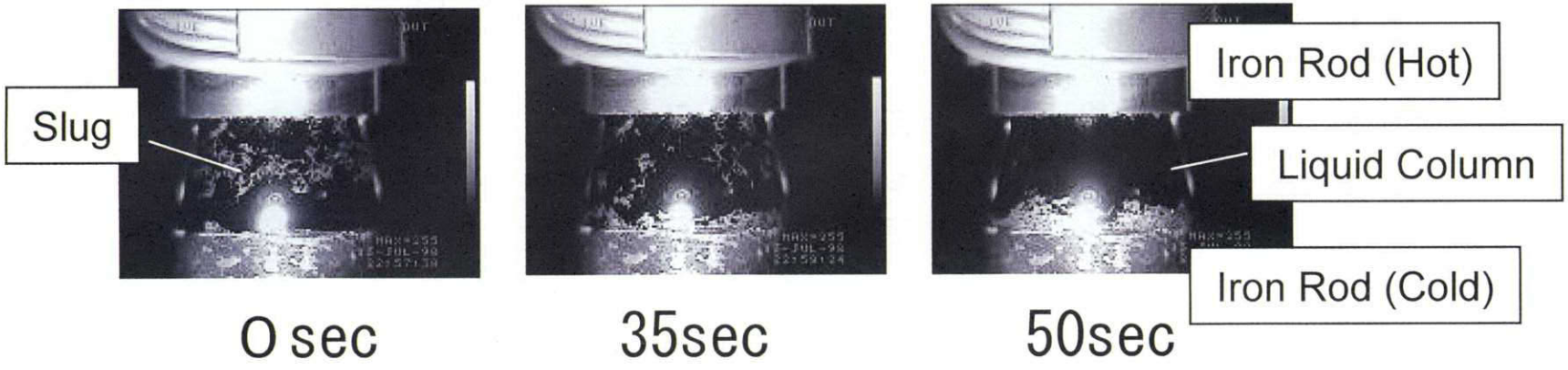

Figure 6-1. Movement of slug

7 Measurement of temperature fluctuation at free surface

We measured the temperature at the free surface by infrared thermal imaging radiometer (IR Imager). Figure 7-1 shows the temperature field on the free surface obtained by IR imager. This figure indicates that, comparatively, the temperature in the white region is high and that in the black region low. The upper and lower iron rods are covered by aluminum foil with low emissivity to reduce the radiant energy. We observed that the surface of the iron rod is at a low temperature. Because we did not calibrate the temperature field based on emissivity on the free surface, temperature values indicated in this figure are proportional to radiant energy at the local point.

We expected that the isothermal temperature was almost parallel to that of the surface of the iron rod, given that the temperature field is mainly governed by thermal conduction. However, we found that the temperature in the middle area is lower than that at the left/right edge areas. This difference is caused by the directional spectral emissivity at the free surface of molten tin. A general description of directional spectral emissivity on polished metal is shown as Fig. 7-2. Spectral emissivity grows with the angle θ measured from the normal of surface in $\theta \leq 80$[deg], and sharply decreases in $\theta \leq 90$[deg]. In the liquid bridge, θ at a local point on the free surface grows from the center toward the edge. Thus, radiant energy from the free surface grows toward the edge of the liquid bridge. That is, we observed that the temperature on the free surface increases toward the edge of the liquid bridge.

We could not obtain a reasonable temperature field, though we could detect temperature fluctuation on the free surface in a portion of the middle area of the liquid bridge.

Figure 7-3 shows temperature fluctuation and FFT analysis of temperature fluctuation at a local point on the free surface. In this case, temperature difference is 20K and the liquid bridge is 10mm in diameter and 4.1mm in height. We observed sinusoidal temperature fluctuation and found two major peaks, 2.8 and 5.6Hz, in FFT analysis. This demonstrates 'period doubling', which is frequently observed as the transition behavior from laminar flow to turbulent flow.

Figure 7-4 shows photographs of temperature fluctuation on the free surface. Figure 7-5 is a diagram illustrating isothermal fluctuation on the free surface. Because we did not obtain a reasonable temperature field, we cannot clarify the physical meaning of this

fluctuation. Temperature fluctuation on free surface requires further investigation.

Measurements under conditions similar to those above were carried out on another day. In this case, the height of the liquid bridge was 4.5mm. Other conditions were equivalent to those in previous measurements. Figure 7-6 shows temperature fluctuation and FFT analysis of temperature fluctuation at a local point on the free surface. We found three major peaks in FFT analysis of temperature fluctuations on the free surface, at frequencies of 0.56, 1.7, and 2.5Hz. We also observed surface fluctuation under these conditions. This fluctuation was recognized by observing the vibration of a light source reflected on the free surface. We obtained a value for the surface fluctuation by analyzing the brightness of the light source. Figure 7-6 shows FFT analysis of surface fluctuation. We can see two major peaks, at 1.5 and 3.2Hz, respectively. There is no apparent relationship between temperature and surface fluctuation.

Additional measurements were conducted to confirm the reproducibility of results of temperature fluctuation. In this case, the height of the liquid bridge was 4.7mm, and temperature difference was 10K. Figure 7-7 indicates temperature fluctuation and FFT analysis of temperature fluctuation at a local point on the free surface. We found two major peaks in FFT analysis of temperature fluctuations on the free surface, at frequencies of 0.71 and 2.5Hz, respectively.

Table 7-1 shows the influence of the height of the liquid bridge on the frequency of temperature fluctuation obtained from our experiments. We did not find a clear tendency in the data presented in this table, and the reproducibility of frequency of temperature fluctuations may not be guaranteed. This is due to oxidation on the free surface of the liquid bridge. Figure 7-8 shows the transition of conditions on the free surface with time. Here, the degree of the vacuum is in the order of 10^{-5} Pa. We observed that the free surface is shiny immediately after forming the liquid bridge, though a thin film gradually covered the free surface. This film, generated by the oxidation that occurs on the free surface, suppresses thermocapillary flow. Further, this oxidation film may reduce the reproducibility of experimental results. Since dissociation pressure is extremely low in molten tin, it is impossible to prevent the oxidation perfectly under the vacuum conditions generated by a vacuum pump. Future experimentation should address the technical problem of extending the duration for which the free surface is not covered with oxidation film.

Comparing our results with those from direct numerical simulation by Prof. Imaishi [10], Table 7-2 shows the minimum frequency by FFT analysis of temperature fluctuation obtained by the present experiments and those obtained by direct numerical simulation. The

difference between minimum frequencies obtained by the present experiment and those obtained by direct numerical simulation is 27%. We suppose that this difference arises from inaccuracies in the experimental results related to the oxidation film. Reproducibility of experimental data must be improved, and more precise data obtained.

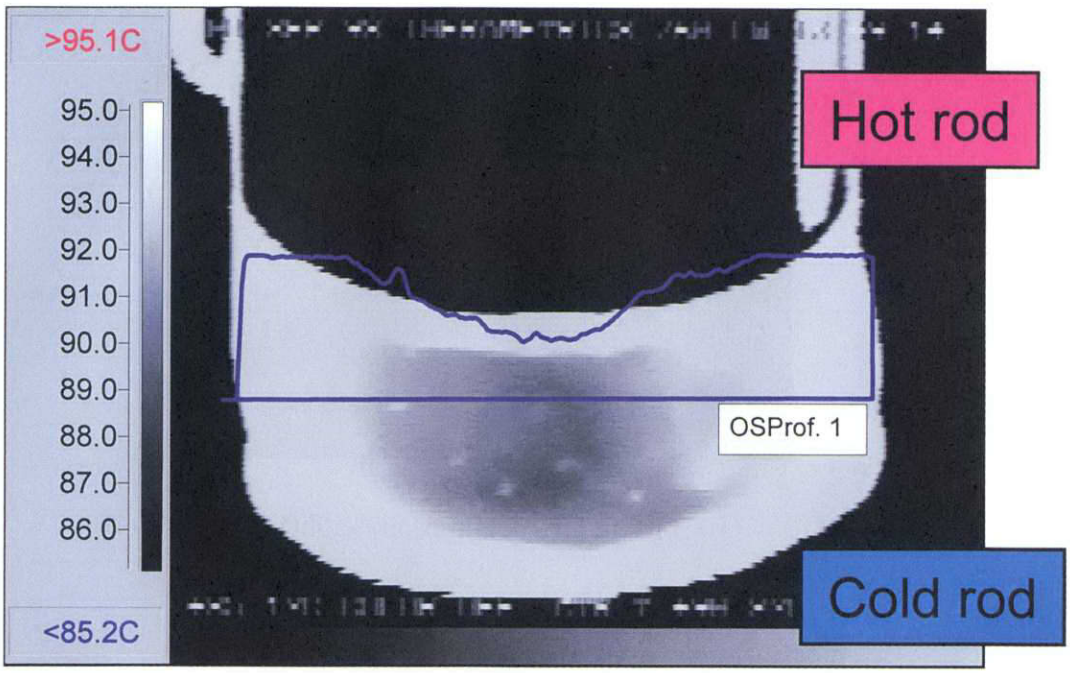

Figure 7-1. Temperature field on the free surface

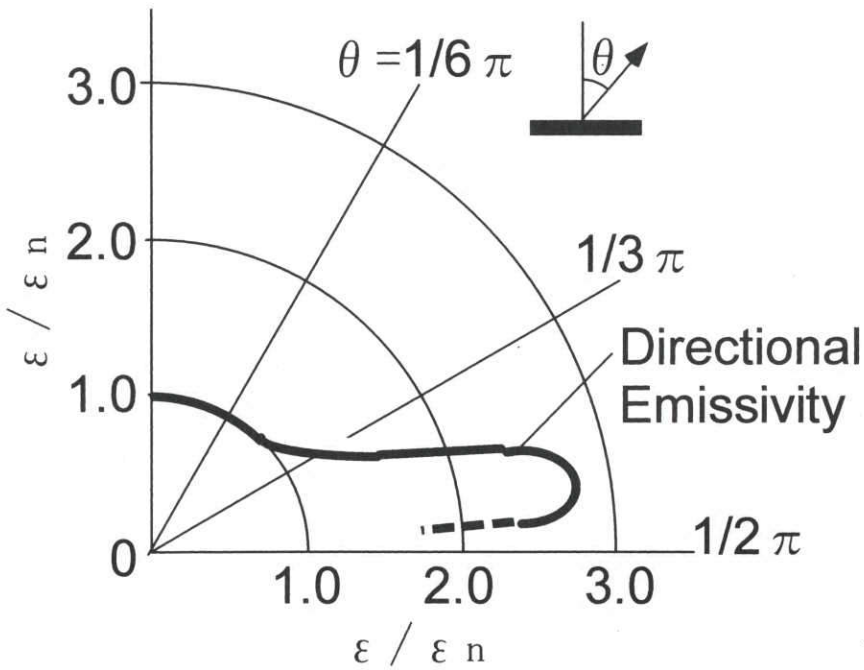

Figure 7-2. Directional spectral emissivity of polished metal

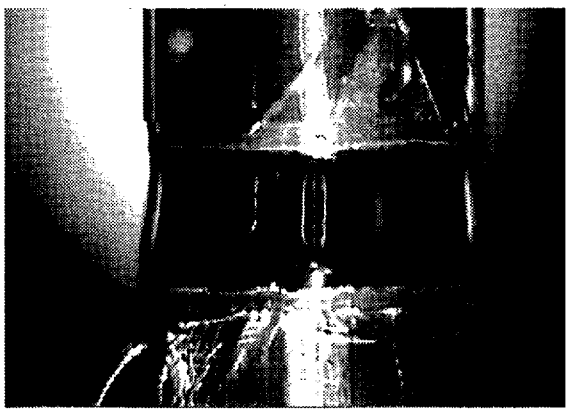

Liquid Bridge
(10[mm] in Dia. 4.1[mm] in height)

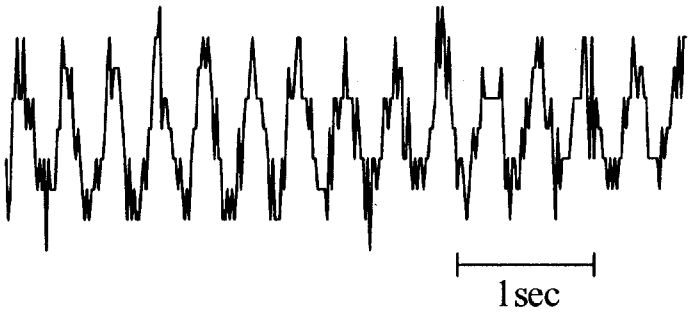

Temperature fluctuation at local point

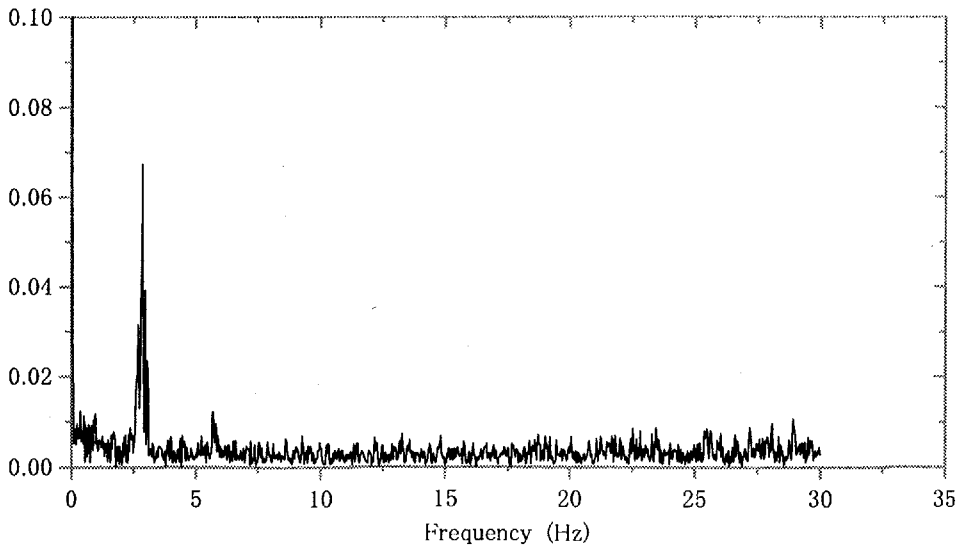

FFT Analysis of temperature fluctuation

Figure 7-3. Temperature fluctuation on the free surface

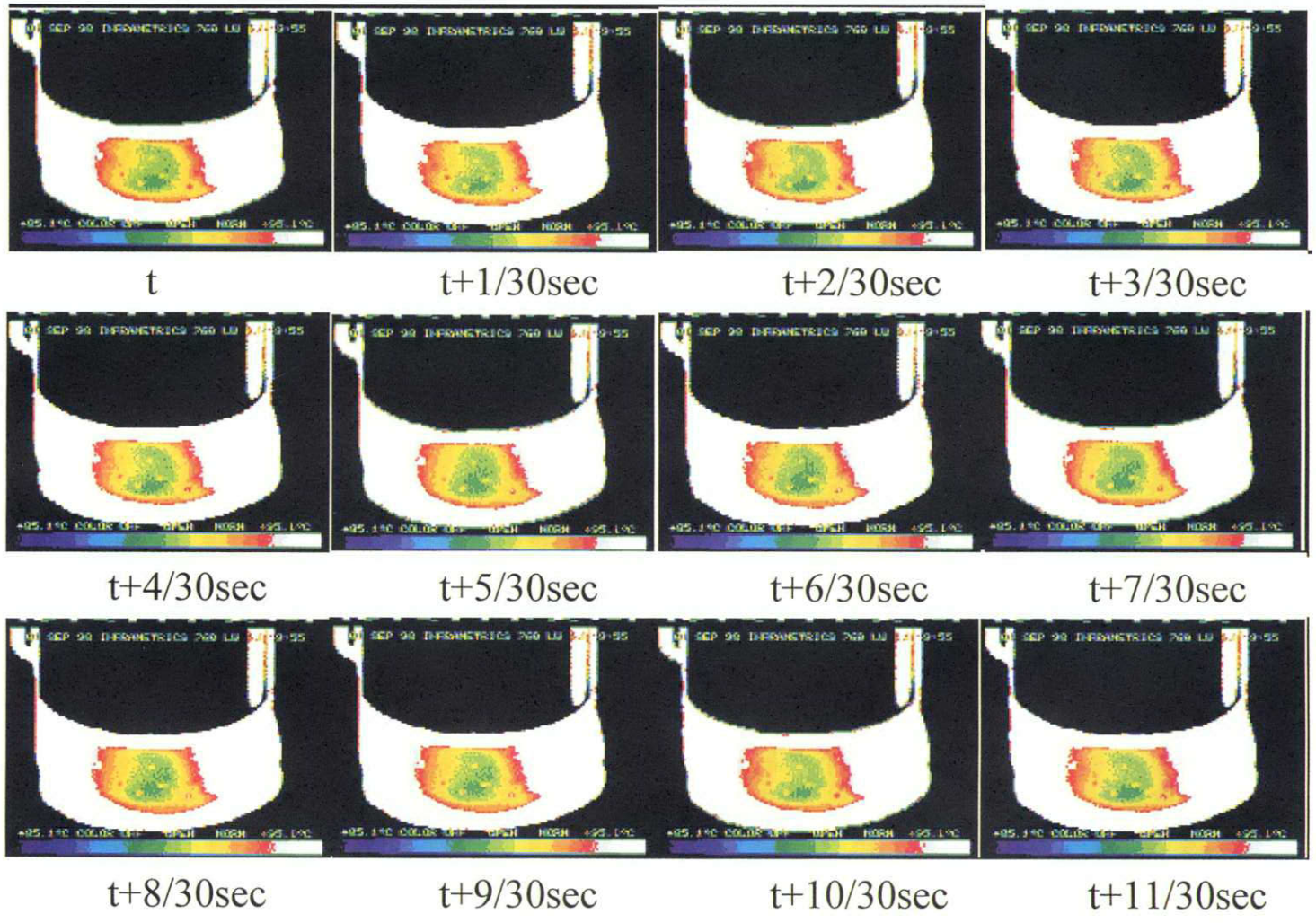

Figure 7-4. Photographs of temperature fluctuation on the free surface

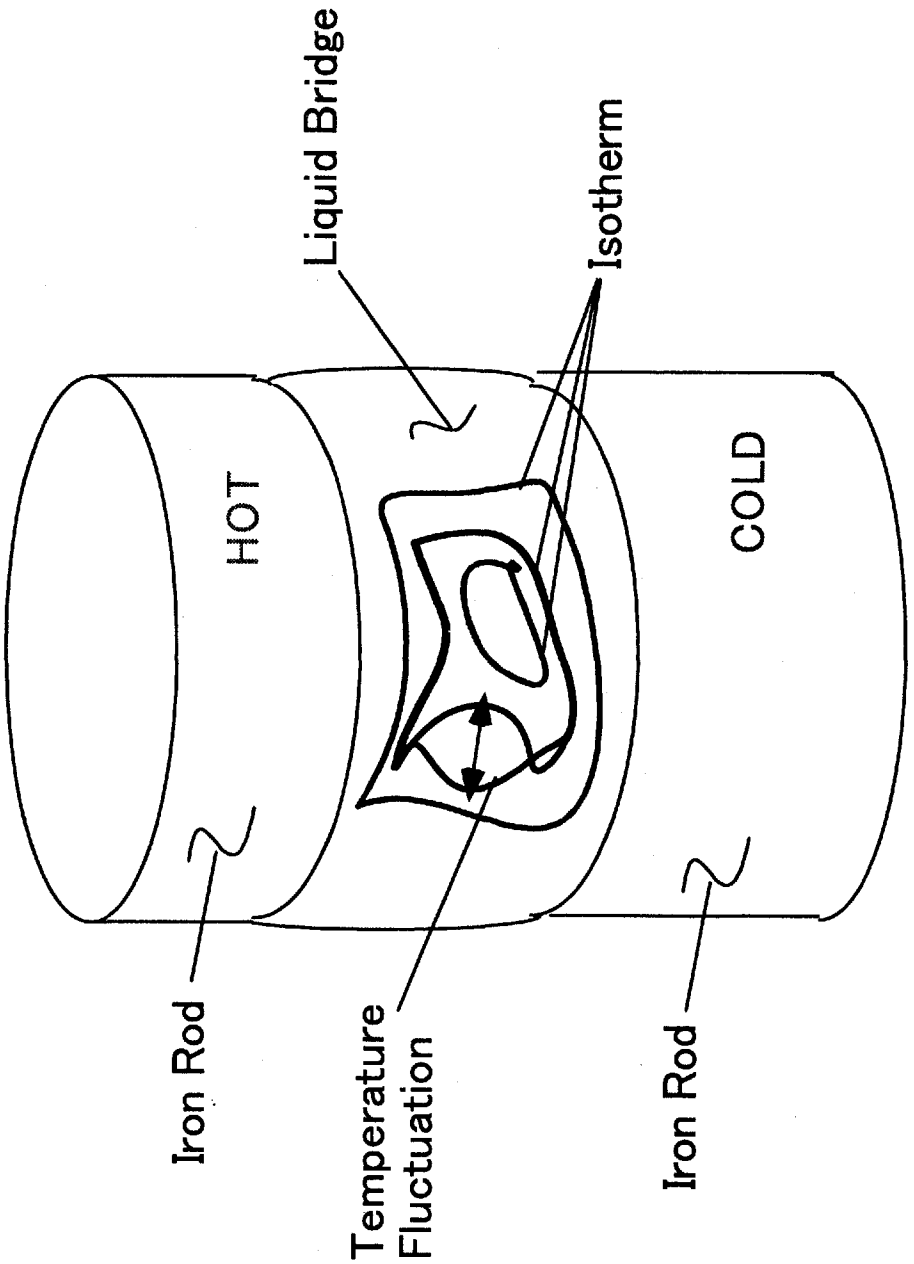

Figure 7-5. General drawing of temperature fluctuation on the free surface

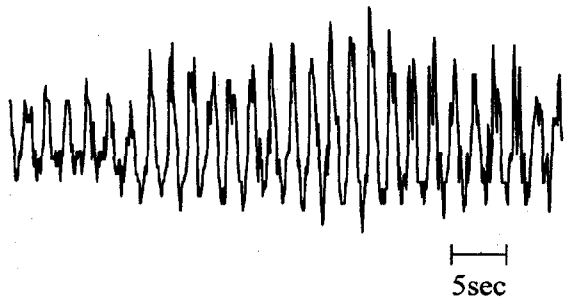

Temp. Fluctuation

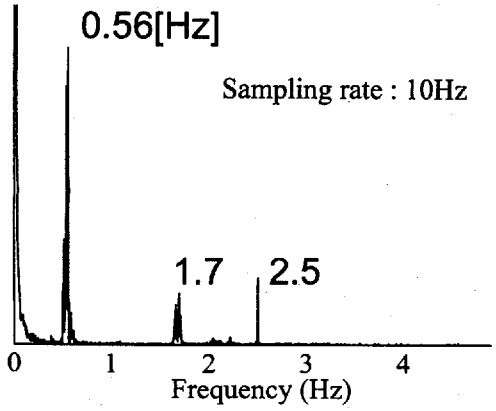

Result of FFT Analysis

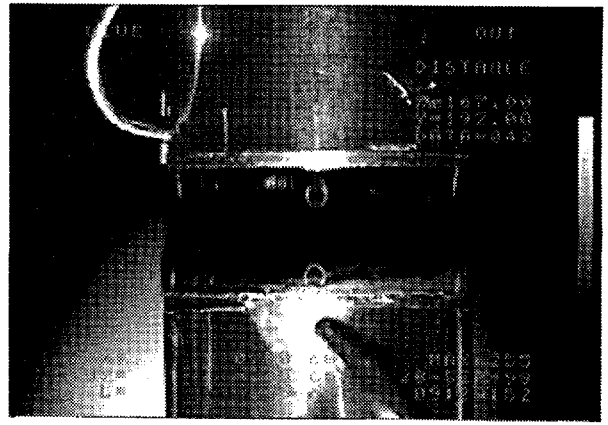

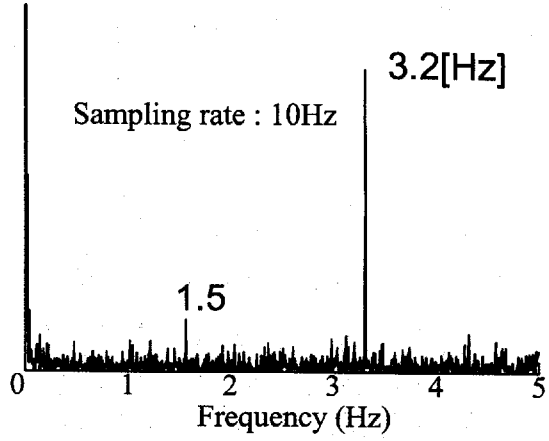

FFT of Surface Fluctuation

Figure 7-6. Temperature and surface fluctuation on the free surface

(10mm in Dia., 4.5mm in Height)

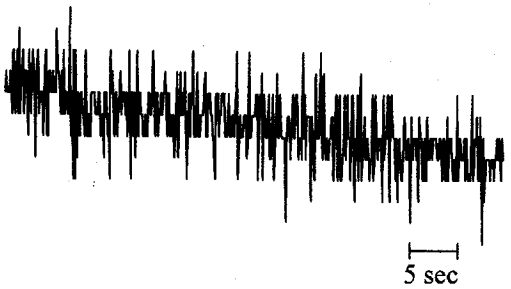

Temp. Fluctuation

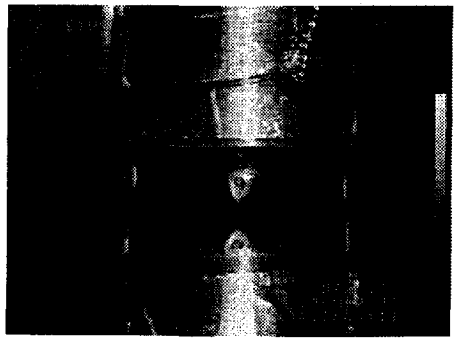

Liquid Bridge

(10mm in Dia., 4.7mm in Height)

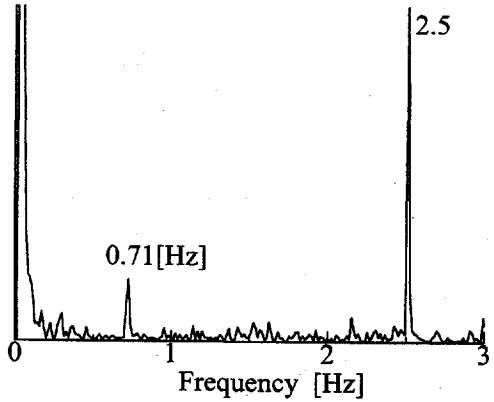

Result of FFT Analysis

Figure 7-7. Temperature and surface fluctuation on the free surface

(10mm in Dia., 4.7mm in Height)

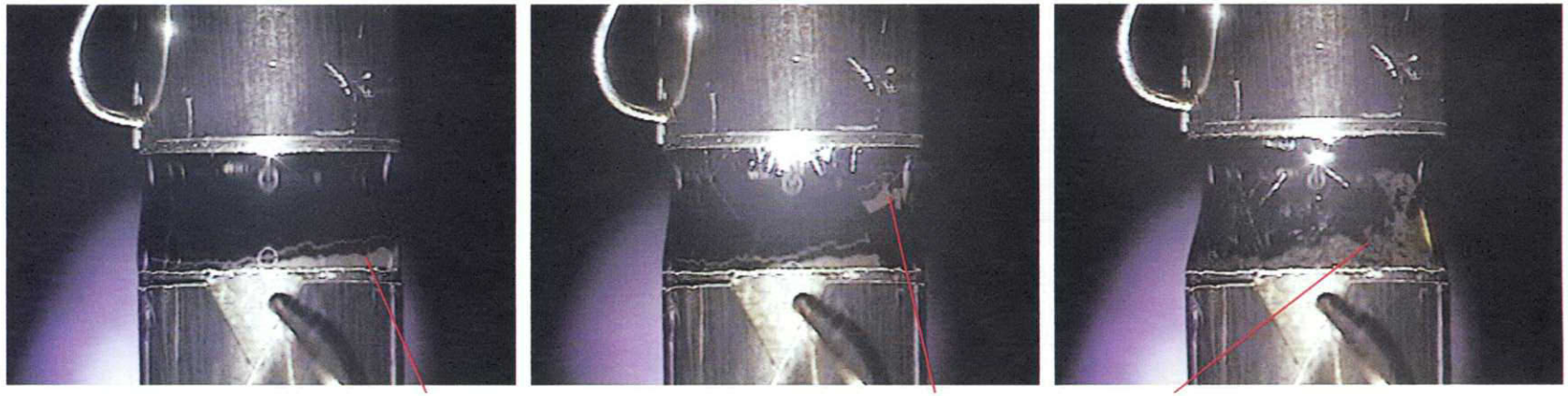

Figure 7-8. Transition of condition on the free surface with time

Table 7-1. Experimental results of temperature fluctuation on the free surface

Diameter [mm]	Height [mm]	Minimum frequency of temperature fluctuation [Hz]
10.0	4.1	2.8
	4.5	0.56
	4.7	0.71

Table 7-2. Comparison between experimental results and direct numerical simulation

	Experimental Results	Direct Numerical Simulation
	Present	Imaishi's Calculation
Prandtl Number Pr	0.0086	0.01
Aspect Ratio As	0.9	1.2
Marangoni Number Ma	224	226
Minimum Frequency of Temperature Fluctuation	**0.56**	**0.44**

8. Open problem

8-1 Further purification to remove residual surface oxides and prevention of oxidation

A method of further purification is required to remove residual surface tin oxides, and a method of preventing oxidation of molten tin during such experiments should be developed in order to allow reproducibility of experimental data. Further, the development of these techniques may extend the duration of the clean surface of molten tin, thus enabling observation of the transition to oscillatory flow.

The throat-capillary method shown in Fig. 4-2 is effective for removal of bulk oxides in molten tin. In order to remove residual surface oxides (seen as a white island in Fig. 7-1), we investigated the application of the Ar^+ ion etching method by using an ion gun designed for surface cleaning. Under the same conditions, the spattering yield of SnO_2 is 2.4 times larger than that of metallic Sn, and the yield of Sn is 1.7 times larger than that of metallic Fe [14], [15]; thus, in our system, it is expected that selective etching of surface tin oxides will proceed.

A high degree of cleanliness in the vacuum chamber is required for prevention of further oxidation of the free surface of molten tin. A quadrupole mass spectrometer with very high sensitivity was installed for monitoring partial pressure of O_2 and H_2O in order to detect trace amounts lost through leaks in the vacuum chamber. A purification system of Ar or H_2 was also installed in order to obtain these gases with ultra high purity. The atmospheric pressure of Ar or H_2 can be conducted by using this system for prevention of further oxidation of tin.

Future research will include study of the effects of adsorbed oxygen on surface tension and its temperature dependence because it is markedly difficult to remove adsorbed oxygen completely. In addition, we will examine a quantitative analytical method of adsorbed oxygen.

8-2 Measurement of the temperature field at the free surface

We could not successfully obtain the temperature field on the free surface by means of the IR imager due to low and directional emissivity of molten tin. We consider that it may be possible to calibrate the observed temperature field by determining the directional emissivity of molten tin prior to measuring the temperature field. However, accurate measurement of directional spectral emissivity of molten tin

presents many difficult technical problems, and the calibrated temperature field will have significant errors. Therefore, we consider measurement of several local temperatures simultaneously by means of optical fiber type radiation thermometers. By this method, the wave number concerning temperature fluctuation could be anticipated by phase differences between each output signal of the thermometer.

8-3 Measurement of flow field in the liquid bridge

Measurement of flow fields is very important for experimental study with low Prandtl number fluids because the velocity vector is not in accord with the isotherms. In general, low Prandtl number fluids are opaque, so only a few techniques are applicable for the measurement of flow fields. One of the available techniques is based on the principle by which the Doppler shift of an ultrasonic wave reflected from moving particles suspended in the fluid is detected [16]; however, this technique provides information essentially about a one-dimensional velocity vector. Recently, an X-ray visualization system has been developed for three-dimensional observation of flow fields in molten silicon [2]. This technique requires that relatively large particles be suspended in the fluid, so the spatial resolution is relatively low, especially for observation of transition to oscillatory flow.

A visualization method using ultrasonic echo signals reflected from moving particles has potential for three-dimensional observation of flow fields with high spatial resolution. As seen in Fig. 8-1, the proposed probe features a multi-piezoelectric vibrator system with a very high Curie temperature. The principle of the method is based on the visual inspection technique under sodium in the experimental Fast Breeder Reactor, but further development to miniaturize the vibrator and to operate at a higher frequency is recommended. Preliminary studies are now underway for the prediction of spatial and time resolution for the measurement of the liquid bridge of tin.

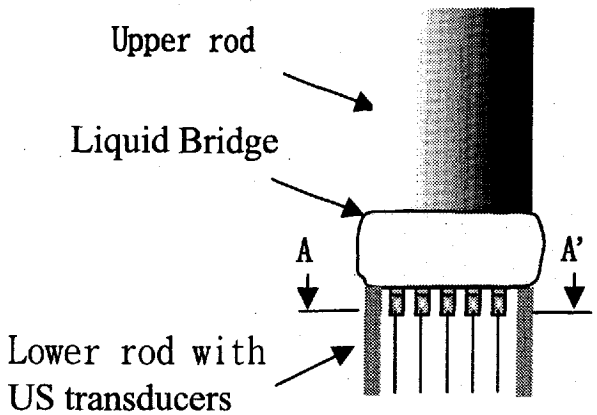

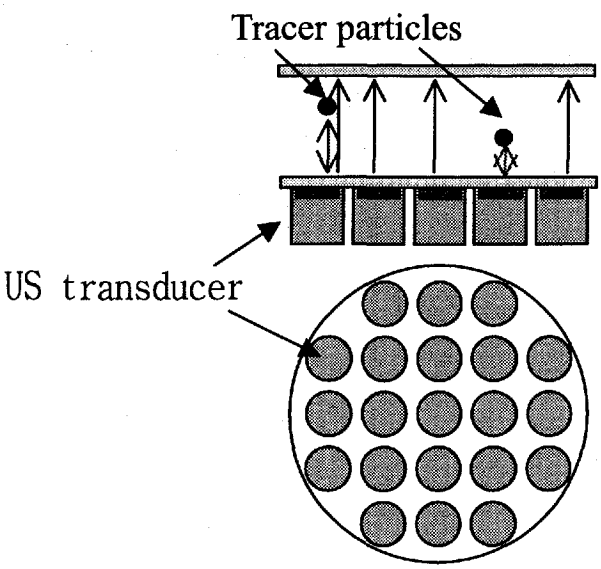

A-A' View

Transducer specifications (target)

Heat resistance	: 770 K
Curie temperature	: 1470 K
Frequency	: >10MHz
Diameter	: <2mm
Material	: $LiNbO_3$ (Lithium niobate)

Figure 8-1. Proposed probe for three-dimensional visualization method using ultrasonic echo signals

9. Conclusions

Temperature fluctuations on the free surface of the molten liquid bridge are measured before detecting the transition point toward oscillatory thermocapillary flow.

We selected molten tin as the liquid substance with a low Prandtl number because of its low melting point and low vapor pressure, and selected pure iron as the holding rod of the liquid bridge based on the measurement results of its wettability.

Thermocapillary flow was confirmed by tracing the slug generated on the free surface under conditions of oxidation, and temperature fluctuations were measured by IR imager. The minimum frequency of temperature fluctuation was 0.56Hz on the liquid bridge of 10mm in diameter and 4.5mm in height at a temperature difference of 20K. However, we did not find a clear tendency or reproducibility concerning the relationship between the height of the liquid bridge and the frequency of temperature fluctuation, which is seemed to be due to these difficulties are caused by oxidation film on the free surface. In future experiments, we intend to address the technical problem of extending the duration for which the free surface is not covered with oxidation film.

10. References

[1] Nakamura, S., Hibiya, T., Kakimoto, K., Imaishi, N., Nishizawa, S., Hirata, A., Mukai, K., Yoda, S., and Morita, T., Journal of Crystal Growth, vol. 29, 1975.

[2] Hibiya T., et al, Marangoni flow of Si melt: Microgravity experiments and perspective, Proc. of Joint 1st Pan-Pacific Basin Workshop and 4th Japan-China Workshop on Microgravity Sciences, 1998.

[3] Han J., Sun Z., Dai L., Xie J., and Hu W., Experiment on the thermocapillary convection of a mercury liquid bridge in a floating half zone, Journal of Crystal Growth, Vol. 169, pp. 129-135, 1996.

[4] Cheng M. and Kou S., Proc. of 4th Microgravity Fluid Physics Conference, 1998.

[5] Kuhlmann H., Hydrodynamic instabilities in thermocapillary Flows, Microgravity Science Technology VII/2, pp75-82., 1994.

[6] Chen G., Lizee A.,and Roux B., Bifurcation analysis of the thermocapillary convection in cylindrical liquid bridges, Journal of Crystal Growth, vol.180, no.3-4, 638-47, 1997.

[7] Rupp R., Müller G., and Neumann G., Three-dimensional time dependent modeling of the Marangoni convection in zone melting configuration for GaAs, Journal of Crystal Growth, vol. 97, 34-41, 1989.

[8] Levenstam M. and Amberg G., Hydrodynamical instabilities of thermocapillary flow in a half zone, Journal of Fluid Mechanics, 297, 357-372.

[9] Leypoldt J., Kuhlmann H., and Rath H., Three-dimensional numerical simulation of thermocapillary flows in cylindrical liquid bridges, Journal of Fluid Mechanics, submitting.

[10] Private communications

[11] Thermophysical properties handbook, Yokendo, 1990.

[12] JSME Handbook Heat Transfer, 4th edition, 1986.

[13] Hassan A., et al, The density and temperature dependence of the surface tension molten bismuth, lead, and bismuth-lead alloys, Zeitshift für Metallkunde, vol. 68, no.6, pp.437-439, 1977 (in German).

[14] Almen O. and Bruce G., Nucl. Instr. Methodes II, pp.257-279,1961.

[15] Kelly R. and Lam N.Q., Redat. Eff., vol.19, 39, 1973.

[16] Takeda Y., Nuclear Technology, vol.79, 120,1987.